Direct aerobic oxidative homocoupling of benzene to biphenyl over functional porous organic polymer supported atomically dispersed palladium catalyst

Yangqing Liu[a], Yu Zhou[a,b,*], Jing Li[a], Qian Wang[a], Qin Qin[a], Wei Zhang[a], Hiroyuki Asakura[c], Ning Yan[b,**], Jun Wang[a,*]

[a] State Key Laboratory of Materials-Oriented Chemical Engineering, College of Chemical Engineering, Nanjing Tech University (Formerly Nanjing University of Technology), Nanjing, 210009, China
[b] Department of Chemical and Biomolecular Engineering, National University of Singapore, 4 Engineering Drive 4, Singapore 117585, Singapore
[c] Department of Molecular Engineering, Graduate School of Engineering, Elements Strategy Initiative for Catalysts & Batteries (ESICB), Kyoto University, Kyotodaigaku Katsura Nishikyo-ku, Kyoto 615-8510, 615-8245, Japan

ARTICLE INFO

ABSTRACT

Synthesis of biphenyl directly from the oxidative coupling of benzene with O_2 as the sole oxident is an atom-efficiency and environmental-friendly route, which is however unattainable as yet due to the most inert nature of sp^2 C—H bond in benzene ring, especially for recyclable heterogeneous catalysis. In this work, single atomic dispersed palladium(II)-porous organic polymer (POP) catalyst with a high loading (>2 wt%) was constructed by anchoring Pd(II) species on the task-specifically designed POP support tethered with carboxyl acid and sulfonic acid groups. It exhibited efficient activity in the heterogeneous aerobic oxidative coupling of benzene with O_2, giving the highest biphenyl yield of 26.1% so far. The high electrophilicity of thus anchored single atomic Pd(II) species is demonstrated, endowing the unprecedentedly maximum turnover number (TON) of 487 and turnover frequency (TOF) of 352 h^{-1} that expletively exceeds 15 and 88 times of previous heterogeneous catalyst. The catalyst can be facilely recycled and reused, and readily extendable to the conversion of other nonactivated arenes into corresponding biaryls. The designing strategy of POP materials developed in the study may provide a platform towards stable single atomic dispersed noble metal species with desirable electrophilicity as efficient catalysts for more sustainable C—C formation-involved organic transformations.

© 2017 Elsevier B.V. All rights reserved.

1. Introduction

As a fundamental transformation, C—C bond formation is widely academically studied and industrially applied in the production of numerous chemicals [1–4]. Transition metal-catalyzed oxidative coupling reaction by the direct C—H activation has attracted great attentions due to its high atom economy and low cost of reactants [5–9]. However, the majority of the catalytic systems rely on the application of high price and low natural abundant noble metals such as palladium (Pd). Fabricating efficient catalyst with high yield,

turnover number (TON), turnover frequency (TOF) and recovery is challengeable towards target reaction.

Heterogeneous catalyst is preferred, but the example for above reaction is scarce and the substrates are limited to electron-rich substrates like alkene and diphenyla-mine [10–14]. Such situations become serious particularly for the nonactivated arenes, among which benzene has the most inert sp^2 C—H bond with the dissociation energy of 110 kcal mol^{-1} [15,16]. Biphenyl is an ubiquitous important building block with numerous applications in agrochemistry, pharmacy, electronics, conductors, polymers, and liquid crystals [17,18]. Pd(II) catalyzed direct oxidative coupling of benzene with O_2 is the most atom efficient, economical and environmental-favorable synthetic pathway [19–22]. Normally, homogeneous Pd(II) catalysts were applied in this reaction with the maximum TON value of 180 (yield: 25.2%) [22]. Up to now, only one heterogeneous Pd(II) catalyst was reported with the yield

of 18.3% and TON of 32 [21]. Unfortunately, this catalyst could not be reused due to the rapid deactivation in the second run.

Recently, atomically dispersed catalysts, including mononuclear metal complexes and single metal atoms anchored on supports, attract increasing attentions by taking the advantages of outstanding performances, such as extremely high atom efficiency, notable activity and well stability [23–33]. For example, single-site Pd(II) supported on 2,2′-bipyridine-grafted periodic mesoporous organosilica exhibited high activity (TON: 128) in the heterogeneous C—H olefination oxidative Heck reactions and could be reused with little loss in activity [25]. However, no such type catalyst is ready for aerobic oxidative coupling of nonactivated arenes to form aryl–aryl bond. The difficulty comes from the inert C—H bond in benzene, the activation of which requires highly electrophilic Pd(II) active sites. Ligands such as pyridine can provide strong affinity towards stable Pd(II) sites but will weaken their electrophilicity [34]. By contrast, weak affinity will result in low loading of Pd(II) species with unfavorable stability. How to make a trade-off between the electrophilicity and stability becomes a bottleneck to fabricate single atomic Pd(II) based heterogeneous catalyst for the activation of C—H bond in benzene.

In order to address this challenge, we develop a new strategy to heterogenize the Pd(II) species in porous organic polymers (POPs) through an ion exchange process. The POPs have tunable chemical composition and porosity, and more importantly, their surface groups can be facilely adjusted by magnifying the monomers in molecular level to achieve required host-guest interaction [35–40]. In this work, we demonstrate how the surface groups of POPs affect the stability, electrophilicity and the catalytic performance of immobilized Pd(II) species. A new POP material tethered with adjacent double —COOH groups and —SO$_3$H groups is constructed (Scheme 1), and atomically dispersed Pd(II) with high electrophilicity are anchored via the interaction with these surface groups in an ion-exchange process, in which the adjacent double —COOH groups can stabilize the anchored Pd(II) species through the formation of unique seven-membered ring structure [41] while the —SO$_3$H groups will further enhance the electrophilicity. The obtained heterogeneous catalyst exhibits efficient activity, superior TON and TOF in the direct oxidative coupling of benzene to biphenyl by using O$_2$ as the sole oxidant. After reaction the catalyst can be facilely separated and reused, which was not possible with previous catalysts. The substrate scope is investigated on other nonactivated arenes to illustrate the versatility of this methodology. To the best of our knowledge, it is the first atomically dispersed Pd(II)-POP catalyst that effectively promotes the oxidative coupling of even the least activated arenes via direct C(sp^2)—H activation.

2. Experimental

2.1. Materials

All reagents were of analytical grade and used as purchased without further purification.

2.2. Preparation of porous organic copolymer

The porous organic copolymer (POP) sample PDMS was prepared through the following steps (Scheme 1). Firstly, the copolymer precursor PDMS-I was prepared through free radical copolymerization by using potassium persulfate (KPS) as the initiator. In detail, maleic anhydride (MA, 0.152 g, 1.55 mmol), sodium p-styrene sulfonate (SS, 0.64 g, 3.1 mmol), divinylbenzene (DVB, 1.21 g, 9.3 mmol) and KPS (0.04 g, 0.15 mmol) were dissolved in a mixed solution of ethanol (20 mL) and water (40 mL). The obtained solution was stirred at 60 °C for 12 h under nitrogen atmosphere.

The white solid was collected by filtration, washed with ethanol and water successively, giving the product PDMS-I. In the second step, PDMS-I was treated by NaOH aqueous solution (0.25 mol/L) at 90 °C for 1 h to generate carboxylate groups from the potential ester groups that formed through the reaction of MA with ethanol during the copolymerization process. The solid PDMS-II was separated by filtration and washed with water. Finally, PDMS-II was treated with aqueous sulfuric acid solution (1 mol L^{-1}). After stirring at room temperature for 24 h, the solid was collected by filtration, washed with water until the filtrate was neutral, and then dried at 80 °C for 12 h. The white solid PDMS (1.2 g) was obtained in 60% yield.
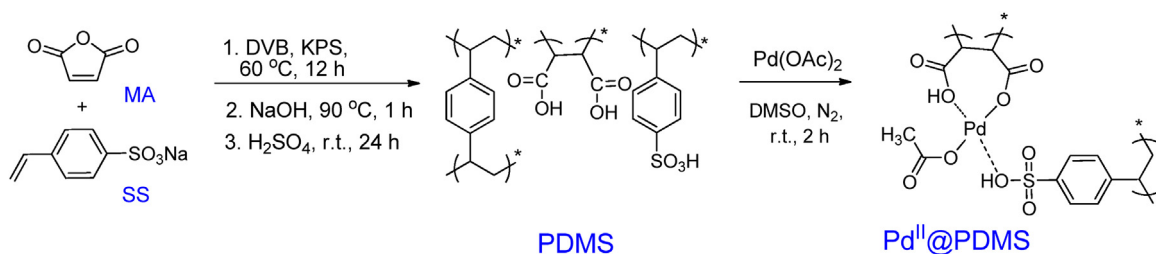
Several other POPs materials were synthesized with a similar procedure by varying the monomers (Scheme S1). They were PDS (copolymer of DVB and SS), PDM (copolymer of DVB and MA), PDAS (copolymer of DVB, acrylic acid (AC) and SS) and PDVB (homopolymer of DVB). Details are seen in the Supporting Information.

2.3. Preparation of Pd^{II}@POPs

Pd(II) loaded sample Pd^{II}@PDMS was prepared through anchoring Pd(II) on the polymer PDMS by using DMSO (dimethyl sulfoxide) as the solvent and Pd(OAc)$_2$ as the precursor [25]. Typically, PDMS (0.1 g) was placed in a 25 mL Schlenk tube and dried under vacuum at 90 °C. After that, 5 mL DMSO solution containing Pd(OAc)$_2$ (0.01 g, 0.045 mmol) was added and the mixture was stirred at room temperature for 2 h under nitrogen atmosphere. The brown solid Pd^{II}@PDMS was collected by filtration, washed with acetone to remove the weak physically adsorbed Pd(OAc)$_2$, and finally dried under vacuum at room temperature for 24 h. The acetic acid amount in the filtrate was analyzed as follows. After the loading process, 1, 4-dioxane (2 μL) was added to the solution as the internal standard. The solid was removed by filtration and the filtrate was analyzed through gas chromatography (GC, Agilent 7890B) equipped with a FID (flame ionization detector) and a capillary column (HP-5, 30 m × 0.25 mm × 0.25 μm). Pd(II) loaded on other POPs were prepared similarly and the obtained products were denoted as Pd^{II}@POP (POP: PDS, PDM and PDAS).

2.4. Characterization methods

Pd K-edge X-ray absorption spectra of Pd^{II}@PDMS and reference materials, Pd foil and Pd(OAc)$_2$, were recorded at the BL01B1 beamline of the SPring-8 (Japan Synchrotron Radiation Research Institute, Hyogo, Japan) in transmission mode at ambient temperature. X-ray energy was calibrated at the inflection point (24350.0 eV) of the absorption edge of Pd metal foil. Data analysis was carried out with Athena and Artemis included in the Demeter package [42]. Fourier transform infrared spectroscopy (FTIR) spectra were recorded on an Agilent Cary 660 instrument (KBr disks) ranging from 4000 to 400 cm^{-1}. Elemental analyses were performed on a CHN elemental analyzer Vario EL cube. The nitrogen sorption isotherms were measured at the temperature of liquid nitrogen (77 K) by using a BELSORP-MINI analyzer with the samples being degassed at 100 °C for 3 h before analysis. The surface area and pore-size distribution curves were calculated by the BET (Brunauer-Emmett-Teller) and BJH (Barrett-Joyner-Halenda) method, respectively. Scanning electron microscopic (SEM) images were viewed on a Hitachi S-4800 field-emission scanning electron microscope. Transmission electron microscopy (TEM) analysis with energy-dispersive X-ray spectrometry (EDS) was conducted on a JEM-2100 (JEOL) electron microscope operating at 200 kV. The X-ray photoelectron spectra (XPS) was conducted on a PHI 5000 Versa Probe X-ray photoelectron spectrometer equipped with Al Karadiation (1486.6 eV). The XPS peaks were systematically analyzed by decomposing the results with the CasaXPS software, using a sum of Gaussian/Lorentzian (80/20) after subtraction of a Shirley-type

Scheme 1. Schematic preparation procedure of Pd^{II}@PDMS.

baseline. Thermogravimetric (TG) analysis was performed with a STA409 instrument in a dry nitrogen atmosphere at a heating rate of 10 °C min^{-1}. Solid state ^{13}C NMR spectra were originally recorded in a Bruker AVANCE-III spectrometer in a magnetic field strength of 9.4 T corresponding to the Larimore frequency of 100 MHz for ^{13}C nuclei with a CP/MAS unit at room temperature. The spinning rate and contact time were 12 KHz and 2.5 ms, respectively. The pulse width, spectral width, and acquisition time was 3.0 μs, 300.0 KHz and 33.91 ms, respectively. For each spectrum, 10000 scans were accumulated. The total amount of carboxylic acid (—COOH) and sulfonic acid (—SO$_3$H) groups on the polymer (n_{total}) was measured by the acid-base inverse titration method using methyl orange as the indicator. The amount of —SO$_3$H groups (n_{SO3H}) was obtained from the elemental analysis. The amount of —COOH groups (n_{COOH}) was calculated from the following formula: $n_{COOH} = n_{total} - n_{SO3H}$. Pd contents in the catalysts were analyzed by inductively coupled plasma with an ICP OPTMA20000 V analyzer.

2.5. Computation details

Density functional theory (DFT) calculations were carried out by using the Gaussian09 program package [43]. Becke's three-parameter hybrid exchange functional with the Lee-Yang-Parr correlation functional (B3LYP) was employed in this study to optimize the geometries of coordinate compound, followed by a frequency analysis to verify that the obtained structure was the local minima on the potential energy surface. The following combination of basis sets was employed in the current study: the LANL2DZ basis set for Pd atom and the 6–31G basis set for the C/S/H/O/F atoms.

2.6. Procedures for the aerobic coupling of arenes

Direct oxidative coupling of benzene to biphenyl with O$_2$ was carried out in a customer-designed temperature controllable pressured stainless steel reactor (25 mL) equipped with a mechanical stirrer. Typically, benzene (1.34 mL, 15 mmol), acetic acid (3 mL), water (2 mL), tri-fluoromethanesulfonic acid (CF$_3$SO$_3$H, 0.1 g, 0.67 mmol) and catalyst (0.036 mol% Pd to benzene) were successively added in the reactor. After the system was flushed with O$_2$, the reactor was charged with 8 atm O$_2$, heated to 120 °C and stirred for 4 h. The products were extracted by the mixture of H$_2$O and CH$_2$Cl$_2$ (1:1 volume ratio). The identification of products was analyzed by GC/MSD (Agilent Technologies 7890B-5977A GC/MSD) equipped with a capillary column (HP-5MS, 30 m × 0.32 mm × 0.25 μm) and a Triple-Axis detector. Quantitative analyses were performed by gas chromatography (GC, Agilent 7890B) equipped with a flame ionization detector and a capillary column (HP-5, 30 m × 0.25 mm × 0.25 μm). The major products of the oxidative coupling of benzene were biphenyl. The detected by-product was phenol produced by the hydroxylation of benzene. Aerobic oxidative coupling of methyl-substituted benzenes were performed similarly by using the target substrate with the major

products of biaryls. The detected by-products were benzaldehyde and benzoic acid generated from the oxidation of the side chain.

Hot filtration test was applied to investigate the heterogeneous nature of Pd^{II}@PDMS catalyst and check whether there existed the Pd leaching to form homogeneous active species. The reaction of benzene was prematurely stopped after heating at 120 °C under O$_2$ (8 atm) for 0.5 h. Solid was separated by filtration. The filtrate was further heated at 120 °C under O$_2$ (8 atm) for another 3.5 h. The products were detected by GC at the reaction time of 1, 2, 3 and 4 h.

In order to test the recyclability in the catalytic system of benzene, the solid catalyst Pd^{II}@PDMS was recovered by filtration after the reaction, washed with acetone and dried under vacuum at room temperature for 24 h. The recovered catalyst was charged to the next run. Both direct recovered and regenerated catalysts were assessed in a three run recycling tests. Regenerated catalyst was obtained by reloading small amount Pd(II) ions on the recovered catalyst through the similar procedure to the preparation of fresh catalyst.
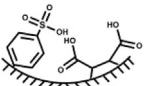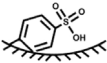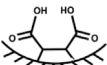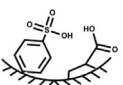
3. Results and discussion

3.1. Fabrication of Pd^{II}@PDMS

The POPs with varied surface groups (Table 1) are synthesized with the procedure in Scheme 1 and S1. XRD patterns (Fig. S1) and N$_2$ sorption experiment (Fig. 1A and S2) indicate that they are all amorphous mesoporous polymers with large surface areas (Table 1). TG analysis reflects that they have well thermal stability with the starting degradation temperature above 400 °C (Fig. S3). SEM images (Fig. S4 and S5) show that they are micrometer-scale irregular blocks, which are composed of aggregated primary particles and exhibit fluffy rough surfaces. The combination of elemental analyses and acid-base inverse titration reveals the chemical composition and the concentration of surface groups (Table S1). Pd(II) species are anchored on these POPs through ion exchange, giving the Pd(II) loaded samples with well-preserved mesoporosity (Table 1, Fig. 1A and S2), thermal stability (Fig. S3) and morphology (Fig. 1B and S5).

The target sample Pd^{II}@PDMS is prepared from the PDMS with adjacent double —COOH (0.86 mmol g^{-1}) and —SO$_3$H (0.47 mmol g^{-1}) groups. ICP analysis indicates that Pd^{II}@PDMS contains a high Pd content of 2.2 wt% (0.2 mmol g^{-1}). Quantitative analysis of acetic acid in the filtrate after ion-exchange in the preparation process shows that about 0.2 mmol g^{-1} acetic acid forms during the anchoring process. This phenomenon implies that the Pd ions are anchored through an ion-exchange process, in which each Pd ion replaces one H$^+$ from the acid groups on PDMS and thereby is bonded to the polymeric framework, with the formation of one molecular acetic acid. TEM image of Pd^{II}@PDMS confirms the mesoporosity and excludes the formation of Pd(0) nanoparticles (NPs) (Fig. 1C). TEM elemental mapping images of O, S and Pd elements (Fig. 1D) demonstrate the existence of SO$_3$H groups and Pd species with homogeneous distribution.

Table 1
Textural properties of various POPs and the corresponding Pd^{II}@POPs.

Entry	Sample	Surface groups[a]	Pd (wt%)[b]	S_{BET} (m^2 g^{-1})[c]	V_p (cm^3 g^{-1})[d]
1	PDMS		–	301	0.28
2	Pd^{II}@PDMS		2.2	255	0.11
3	PDS		–	378	0.62
4	Pd^{II}@PDS		0.4	312	0.47
5	PDM		–	466	0.24
6	Pd^{II}@PDM		2.5	389	0.18
7	PDAS		–	390	0.46
8	Pd^{II}@PDAS		2.4	359	0.26

[a] Surface functional groups on the sample.
[b] Pd content in the Pd^{II}@POPs detected by ICP.
[c] BET surface area of the sample.
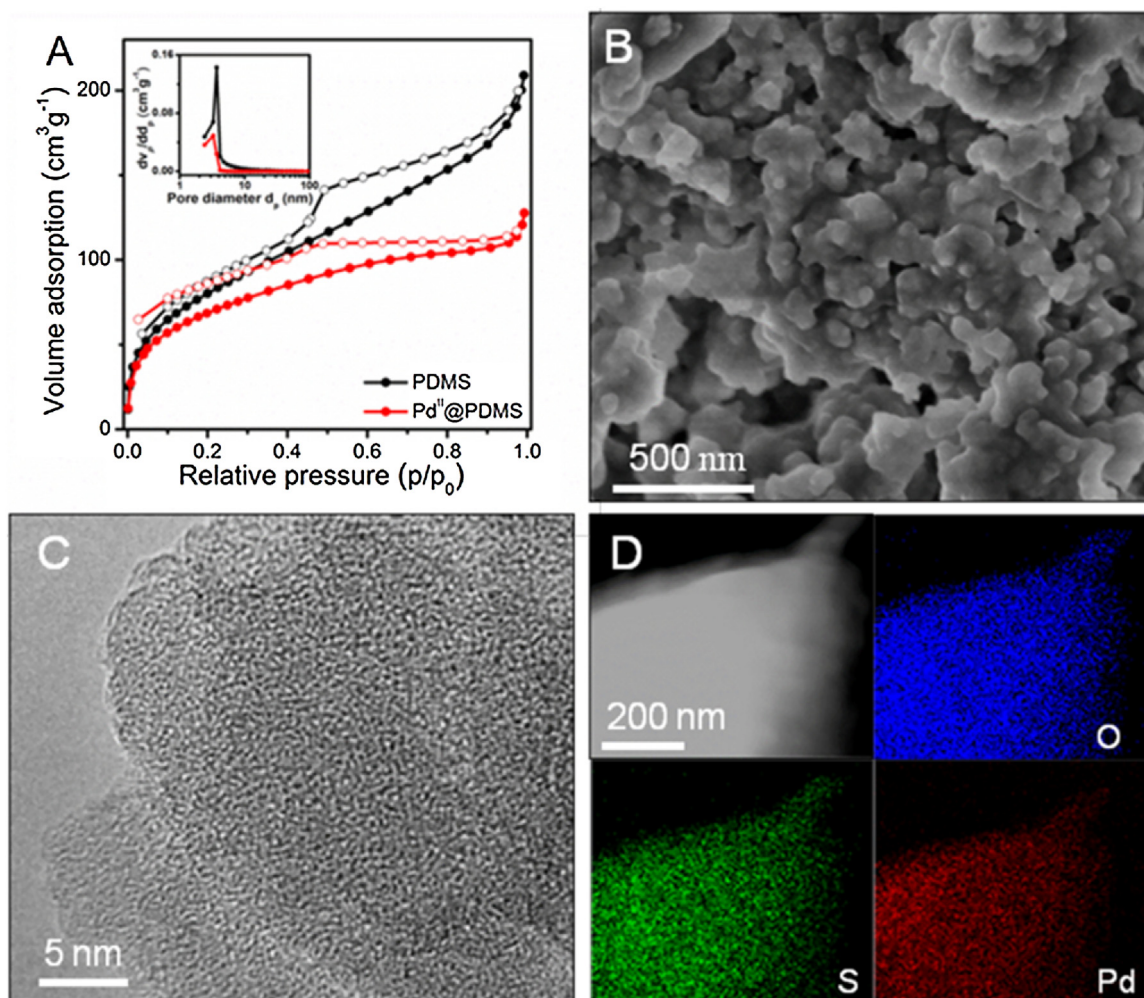[d] Total pore volume of the sample.

Fig. 1. (A) N$_2$ sorption isotherms and pore-size distribution curves (inset) of PDMS and Pd^{II}@PDMS; (B) SEM image of Pd^{II}@PDMS; (C) TEM image of Pd^{II}@PDMS; (D) EDS mapping images for O, S and Pd elements of Pd^{II}@PDMS.

X-ray absorption spectroscopy (XAS) is applied to verify the chemical state and coordination environment of Pd species in Pd^{II}@PDMS. Fig. 2A shows the X-ray absorption near edge structure (XANES) spectra at the Pd K edge of Pd^{II}@PDMS with reference materials Pd foil and Pd(OAc)$_2$. The energy (E$_0$) values of the absorption edge for Pd^{II}@PDMS, Pd(OAc)$_2$ and Pd foil are 24355.5, 24357.0, and 24354.6 eV, respectively. This result reflects that the chemical state of Pd species in Pd^{II}@PDMS is in cationic state but different from the common divalent state like Pd(OAc)$_2$. Extended X-ray absorption fine structure (EXAFS) analysis can provide vital
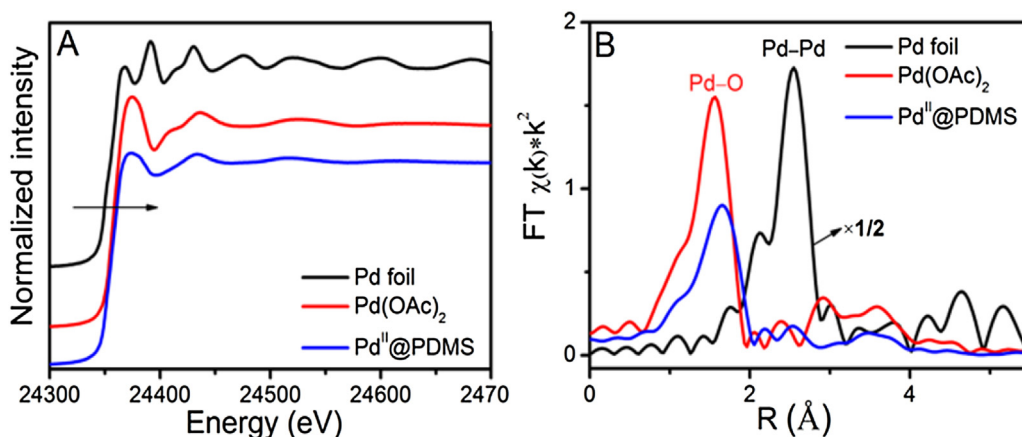
Fig. 2. (A) The normalized XANES spectra at the Pd K-edge of Pd^{II}@PDMS with reference materials Pd foil and $Pd(OAc)_2$; (B) Fourier-transformed spectra of k^2-weighted Pd K-edge EXAFS of Pd^{II}@PDMS with reference materials Pd foil and $Pd(OAc)_2$.

evidences on the dispersion [44,45]. Fig. 2B and S6 displays the Fourier-transformed k^2-weighted EXAFS spectra at the Pd K edge of Pd^{II}@PDMS, Pd foil and $Pd(OAc)_2$. Pd^{II}@PDMS only presents one prominent shell at 1.6 Å mainly derived from the Pd–O contribution. There is no obvious peak in the region 2–3 Å from the Pd–Pd contribution, strongly confirming that Pd species in Pd^{II}@PDMS exist predominantly as isolated sites. These results validate the atomically dispersion of Pd(II) species in Pd^{II}@PDMS.

The solid state ^{13}C NMR, FTIR and XPS spectra further reveal the chemical composition and the existence of −COOH and −SO_3H groups on PDMS and Pd^{II}@PDMS (the signal assignments are summarized in Table S2-S4). As analyzed by the solid state ^{13}C NMR spectra (Fig. 3A), Pd^{II}@PDMS exhibits the similar chemical framework structure as PDMS, suggesting the well-preserved polymeric framework. In the FT-IR spectrum (Fig. 3B), Pd^{II}@PDMS displays weakened peak at 1719 cm^{-1} and a new peak at 1673 cm^{-1}, reflecting the formation of −COO$^-$−Pd^{2+} species derived from the interaction of −COOH groups on the PDMS with $Pd(OAc)_2$ [46]. Such phenomena manifest that Pd(II) ions are mainly anchored through the interaction with the −COOH groups and weakly interact with the −SO_3H, as demonstrated by a small peak emerged at 957 cm^{-1} [47]. Similar result can be obtained by XPS analysis (Fig. 4). The S2p XPS signal shifts from 169.2 for PDMS to 168.9 eV for Pd^{II}@PDMS, reflecting a weak interaction between Pd(II) ions and −SO_3H groups. The O1s spectrum is fitted with five peaks at 531.2 (C−O), 532.1 (SO_3H), 532.9 (C−O−Pd), 533.6 (C=O) and 535.0 eV (SO_3Pd), further reflecting the interaction of Pd(II) with the −COOH and −SO_3H groups to form −COO$^-$−Pd^{2+} and −SO_3^-···Pd^{2+} structure (···denotes a weak and long distance interaction). Pd^{II}@PDMS illustrates two Pd(II)3d peaks at 337.7 ($3d_{5/2}$) and 342.9 eV ($3d_{3/2}$). No peaks corresponding to Pd(0) are found, meaning that the surface Pd species are in Pd(II) state.

Based on above characterizations, the proposed coordination environment is presented in Scheme 1. Atomically dispersed Pd(II) ions are three-coordinated with two −COO$^-$ groups and one −COOH, and the surface −SO_3H groups are weakly interact with anchored Pd(II) ions to form −SO_3^-···Pd^{2+} structure. The numbers of −COOH, −SO_3H and Pd(II) species on the surface of Pd^{II}@PDMS are 2, 1.06, and 0.47 per square nm, respectively. The distance between these groups enables the co-interaction of these groups with the immobilized Pd(II) ions.

During the anchoring process, the surface acid groups play a dominate role in the formation of the stable and highly eletrophilic Pd(II) species. Pd content is undetectable on the final solid by using PDVB without any surface acid groups, suggesting that Pd(II) ions cannot be anchored through merely weak physical adsorption. By

contrast, Pd(II) can be anchored on PDS, PDM and PDAS to afford corresponding Pd^{II}@POPs. FTIR and XPS analyses also show the interaction between Pd(II) ions with the surface −SO_3H or −COOH groups to form −SO_3^-···Pd^{2+} or −COO$^-$−Pd^{2+} in these samples (Fig. S7–S10). The Pd contents of Pd^{II}@PDM and Pd^{II}@PDAS are 2.5 and 2.4 wt%, respectively, close to the one of Pd^{II}@PDMS; whereas Pd^{II}@PDS only contains 0.4 wt% Pd despite the high content of −SO_3H groups (1.95 mmol g^{-1}), implying the weak interaction between Pd species and −SO_3H groups. These phenomena confirm the importance of −COOH groups in immobilizing Pd(II) ions and also show that the weak interaction between Pd(II) ions and −SO_3H groups alone cannot efficiently immobilize Pd(II) ions. Evident Pd(0) species are observed on Pd^{II}@PDS and Pd^{II}@PDAS, as demonstrated by the deconvolution of Pd XPS spectra (Fig. S10, Table S4), in agreement with TEM images (Fig. S11A–B); however, owing to the low Pd content of Pd^{II}@PDS, its TEM image shows no apparent Pd NPs. By contrast, no Pd(0) species form on Pd^{II}@PDM though with a high Pd content (Fig. S10 and S11C, Table S4). These results further demonstrate that the Pd^{II} ions interacting with the adjacent double −COOH groups in MA repeating units can constitute unique seven-membered ring structure to stabilize Pd(II) species. Neither single −COOH nor −SO_3H has such function. Moreover, compared with the Pd(II) BE values of Pd^{II}@PDMS, the ones of Pd^{II}@PDM shift negatively by 0.5 eV, indicating that the electrophilicity of Pd(II) in Pd^{II}@PDM is lower than that in Pd^{II}@PDMS. The Pd(II) BE values of Pd^{II}@PDAS are similar to Pd^{II}@PDMS, indicating the formation of Pd(II) species with the similar electrophilicity. The variation of Pd(II) BE values shows that the surface −SO_3H groups can promote the electrophilicity of immobilized Pd(II) ions. The above results demonstrate the crucial role of surface groups towards highly electrophilic and stable Pd(II) species. The support PDMS reaches the Pd^{II}@PDMS with the surface Pd species in Pd(II) state, thanks to the special stabilization effect of adjacent double −COOH groups and the promotion of surface −SO_3H groups on the electrophilicity through a weak interaction.

3.2. Catalytic activity

The catalytic performance of Pd^{II}@PDMS is investigated in the oxidative coupling of benzene to biphenyl with O_2 (Table 2). The reaction does not proceed in the absence of catalysts or catalyzed by PDMS (entries 1–2). A high yield of 26.1% with selectivity of 98.3% for biphenyl is obtained by using Pd^{II}@PDMS as a heterogeneous catalyst (entry 3). In this process, only small amount catalyst (Pd, 0.036 mol% based on benzene) is involved, giving a high TON of 363. Both the yield and TON over Pd^{II}@PDMS exceed the ones over
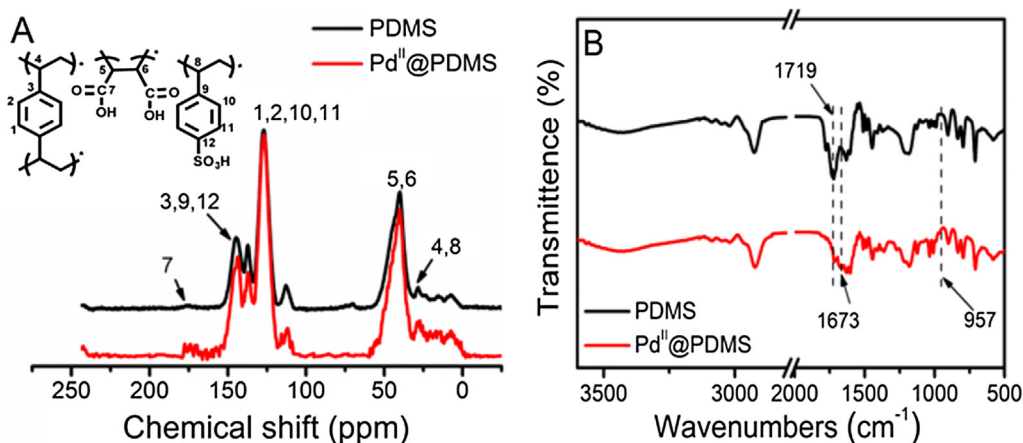
Fig. 3. (A) Solid ^{13}C CP/MAS NMR and (B) FT-IR spectra of PDMS and Pd^{II}@PDMS.

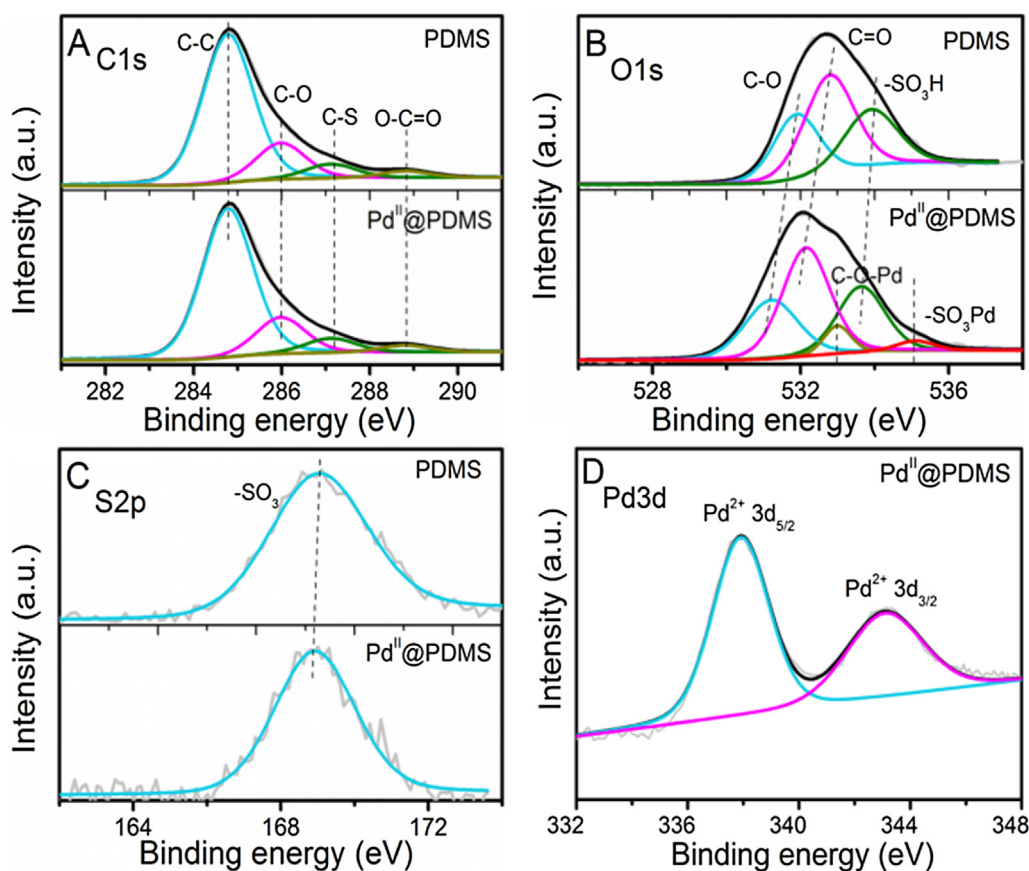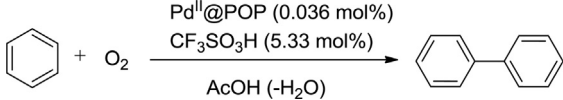**Fig. 4.** (A) C1s, (B) O1s, (C) S1s and (D) Pd3d XPS spectra of PDMS and Pd^{II}@PDMS.

the homogeneous Pd(OAc)$_2$ (yield: 15.3%; TON: 212) and previous heterogeneous catalyst [(C$_3$CNpy)$_2$Pd(OAc)$_2$]$_2$HPMoV$_2$ (yield: 10.4%; TON: 144) under the same reaction condition (entries 6–7). On the other hand, Pd^{II}@PDAS gives low activity with 11.9% yield of biphenyl and TON of 165 (entry 8), which can be ascribed to the existence of Pd(0) species (about 18% according to the XPS analysis, Table S4) that are not the active species for aerobic oxidative coupling reactions [48,49]. The weak interaction between Pd(II) species and −SO$_3$H groups on PDS causes the formation of large amount Pd(0) species (25% according to the XPS analysis, Table S4) and weak stability of immobilized Pd(II) species. Therefore, the obtained catalyst Pd^{II}@PDS only behaves 0.2% yield of biphenyl with TON of 3 (entry 9). Pd^{II}@PDM produces 14.2% yield of biphenyl and

TON of 197 due to the relatively low electrophilicity of Pd(II) ions (entry 10). These observations demonstrate the efficient performance of Pd^{II}@PDMS in this reaction and emphasize the importance to achieve the active immobilized Pd(II) species by modulating the surface groups of POPs.

Various reaction conditions for Pd^{II}@PDMS catalyzed oxidative coupling of benzene to biphenyl with O$_2$ are investigated in details (Fig. S12). The yields as the function of the catalyst amount, reaction time, reaction temperature or O$_2$ pressure exhibit the "volcanic" type curve. The decline of the activity under elevated condition can be assigned to the over-oxidation of the product along with the reaction. Exploration of the catalyst amount reaches an unprecedented TON value of 487 by using only much low Pd amount (0.018

Table 2
Catalytic performances of various catalysts in the aerobic oxidative coupling of benzene to biphenyl.[a]

$$\text{benzene} + O_2 \xrightarrow[\text{AcOH (-H}_2\text{O)}]{\substack{\text{Pd}^{II}@\text{POP (0.036 mol\%)} \\ \text{CF}_3\text{SO}_3\text{H (5.33 mol\%)}}} \text{biphenyl}$$

Entry	Catalyst	Catalysis type	Yield (%)[b]	Sel. (%)[c]	TON[d]	TOF(h^{-1})[e]
1	none	–	0	–	–	–
2	PDMS	hetero	0	–	0	0
3	Pd^{II}@PDMS	hetero	26.1/25.3[i]/23.4[j]	98.3/98.5[i]/98.2[j]	363/351[i]/325[j]	91/88[i]/81[j]
4[f]	Pd^{II}@PDMS	hetero	17.5	98.6	487	122
5[g]	Pd^{II}@PDMS	hetero	12.7	98.3	176	352
6	Pd(OAc)$_2$	homo	15.3	98.5	212	53
7[h]	[(C$_3$CNpy)$_2$Pd(OAc)$_2$]$_2$HPMoV$_2$	hetero	10.4	97.9	144	36
8	Pd^{II}@PDAS	hetero	11.9	98.6	165	41
9	Pd^{II}@PDS	hetero	0.2	98.4	3	1
10	Pd^{II}@PDM	hetero	14.2	98.6	197	49

[a] Reaction conditions: benzene (15 mmol), Pd^{II}@POPs (Pd, 0.036 mol% based on benzene), CF$_3$SO$_3$H (0.12 g, 5.33 mol%), acetic acid (3 mL), H$_2$O (2 mL), O$_2$ (8 atm), 120 °C, 4 h.

[b] Biphenyl yield (%) = 2 × mmol biphenyl/mmol initial benzene.

[c] Biphenyl selectivity (%) = 2 × mmol biphenyl/(2 × mmol biphenyl + mmol phenol).

[d] Turnover number (TON) = mmol biphenyl/mmol Pd.

[e] Turnover frequency (TOF) = mmol biphenyl/mmol Pd/time (h).

[f] Reaction condition: Pd^{II}@PDMS (Pd, 0.018 mol% based on benzene).

[g] Reaction condition: 0.5 h.

[h] Previous heterogeneous catalyst [21].

[i] 2nd run.

[j] 3rd run.

mol% based on benzene) with the biphenyl yield still in high level of 17.5% (Table 2, entry 4). Such high TON value is more than 15 times of the one (TON: 32) over previous heterogeneous catalyst at its highest yield of 18.3% [21]. The investigation of the reaction time shows that an extremely high turnover frequency (TOF) up to 352 h^{-1} reaches at 0.5 h (Table 2, entry 5), which is about 88 times of the one over previous heterogeneous system [21]. The TOF value still locates at a high level of 91 h^{-1} at the highest yield and 122 h^{-1} in the case of the highest TON. Here, in the aerobic oxidative coupling of inert benzene, Pd^{II}@PDMS demonstrates much high TON and TOF values, which are the highest so far for this reaction (Table S5) and even higher than or at least comparable to other homogeneous Pd(II) catalyzed coupling systems [8,50] thanks to the high efficiency of atomically dispersed catalyst and the unique Pd(II) structure.

In order to insight into the heterogeneous nature of Pd^{II}@PDMS, hot filtration test is performed and displayed in Fig. S12B. The result shows that no further product forms if the solid catalyst is removed. This confirms that the conversion process happens on the solid surface and the contribution of the leached Pd species is excluded. After reaction, Pd^{II}@PDMS can be facilely separated by filtration and reused in the next run. The catalyst can be reused at least for three times (23.5% and 20.7% yield for the 2nd and 3rd run, respectively), which was impossible in the previous studies. As demonstrated by the XPS spectrum (Fig. S13) and ICP analysis of the reused catalyst (the Pd content is 1.8 and 1.5 wt% of the recovered catalyst after the 2nd and 3rd run, respectively), the gradually declined activity with consecutive runs comes from the decreased Pd content in the solid and the formation of certain Pd(0) species. IR and nitrogen sorption experiments reveal the preservation of polymeric network and porosity during the recycling (Fig. S14 and S15). By reloading Pd(II) species, improved reusability is achieved (Table 2, entry 3). The yield of biphenyl for each cycle is promoted and remains at 23.4% in the 3rd run, giving a total TON value of 1039 in these three cycles. The slight decreased yield results from the inevitable formation of Pd(0) species (Fig. S16).

The scope of Pd^{II}@PDMS is further extended to the aerobic oxidative coupling of methyl-substituted benzenes (Table 3). The coupling of toluene performs 30.5% yield to dimethylbiphenyl with
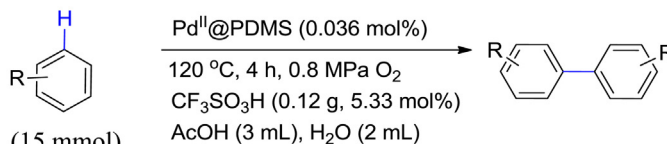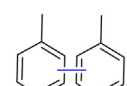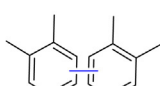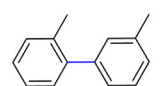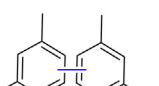
high selectivity of 97.6%, superior TON of 428 and TOF of 107 h^{-1}. The higher activity over toluene than benzene can be assigned to the electron-donating effect of the methyl group. Similarly, o-xylene is also converted into tetramethylbiphenyl in good activity with high yield, selectivity, TON and TOF of 27.6%, 92.1%, 383, and 96 h^{-1}, respectively. Furthermore, Pd^{II}@PDMS can catalyze the conversion of m-xylene and p-xylene into corresponding tetramethylbiphenyl with moderate yields of 25.4% (TON: 353; TOF: 88 h^{-1}) and 10.3% (TON: 143; TOF: 36 h^{-1}), despite the steric effects of the methyl groups. All of these further confirm that Pd^{II}@PDMS is efficient for the activation of nonactivated arenes in the aerobic oxidative coupling, giving high TON and TOF values.
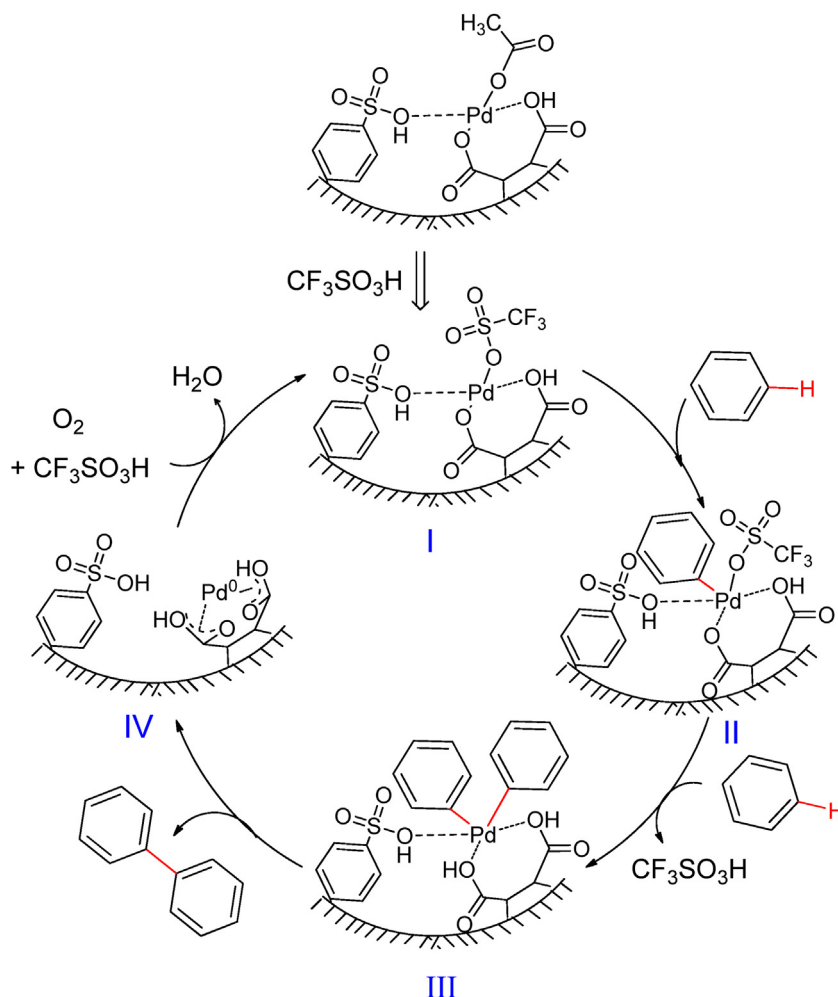
3.3. Understanding of the catalytic process

A heterogeneous catalytic route in Scheme 2 is proposed by combining the catalytic results and previous mechanism studies [51,52]. Firstly, the substrate benzene diffuses towards the solid surface and then accesses the active sites Pd(O$_3$SCF$_3$)$^+$ species (I), in-situ-generated from the interaction of Pd(OAc)$^+$ with CF$_3$SO$_3$H (XRF analysis of the recovered catalyst verifies the existence of F element with the (O$_3$SCF$_3$)$^+$ amount of 0.2 mmol g^{-1}, suggesting that almost all the (OAc)$^+$ is replaced with (O$_3$SCF$_3$)$^+$). The intermediate σ-arylpalladium(II) (II) forms by electrophilic substitution, and then interacts with another benzene to generate biphenyl-Pd(II) species (III). Biphenyl is produced through the reductive elimination of (III) and desorbed from the surface. The formed Pd^0 species (IV) is oxidized with O$_2$ in the presence of CF$_3$SO$_3$H to regenerate the original Pd(II) state (I).

According to this route, the remarkable performance of Pd^{II}@PDMS is assignable to the atomically dispersed Pd(II) ions in the surface of mesoporous polymeric framework. The abundant mesoporosity improves the mass transfer in this heterogeneous catalysis process, and the polymeric network enables well organic compatibility for the facile accessibility of organic compound. The anchored Pd(II) species are highly electrophilic, thus can efficiently activate the nonactivated arenes. The task-specifically designed polymeric matrix PDMS plays a key role in the immobilization of Pd(II) ions with high activity and relatively good stability. The

Table 3
Aerobic oxidative coupling of various methyl-substituted benzenes catalyzed by Pd[II]@PDMS.

Product:				
Yield[a]:	30.8%	27.6%	25.4%	10.3%
Selective[b]:	97.6%	92.1%	91.6%	90.8%
TON[c]:	428	383	353	143
TOF[d]:	107 h^{-1}	96 h^{-1}	88 h^{-1}	36 h^{-1}

[a]Biaryl yield (%) = 2 × mmol biaryl/mmol initial substrate. [b]Biaryl selectivity (%) = 2 × mmol biaryl/(2 × mmol biaryl + mmol aldehydes + mmol carboxylic acids). [c]Turnover number (TON) = mmol biaryl/mmol Pd. [d]Turnover frequency (TOF) = mmol biaryl/mmol Pd/time (h).

Scheme 2. Proposed catalytic cycle for the Pd[II]@PDMS-catalyzed aerobic oxidative coupling of benzene to biphenyl.

surface —COOH groups provide the necessary driving force to anchor the Pd(II) ions. Compared with the ligands such as pyridine, the —COOH groups weakly coordinate with Pd(II) ions, enabling appropriate electron-donating effect that will not restrain the electrophilic substitution of Pd(II) with benzene. The —SO$_3$H groups

have an electron-withdrawing effect on Pd(II) species and facilitate the electrophilic substitution by enhancing their electrophilic property. Moreover, the unique seven-membered ring structure formed from adjacent —COOH groups with Pd(II) can further stabilize sin-
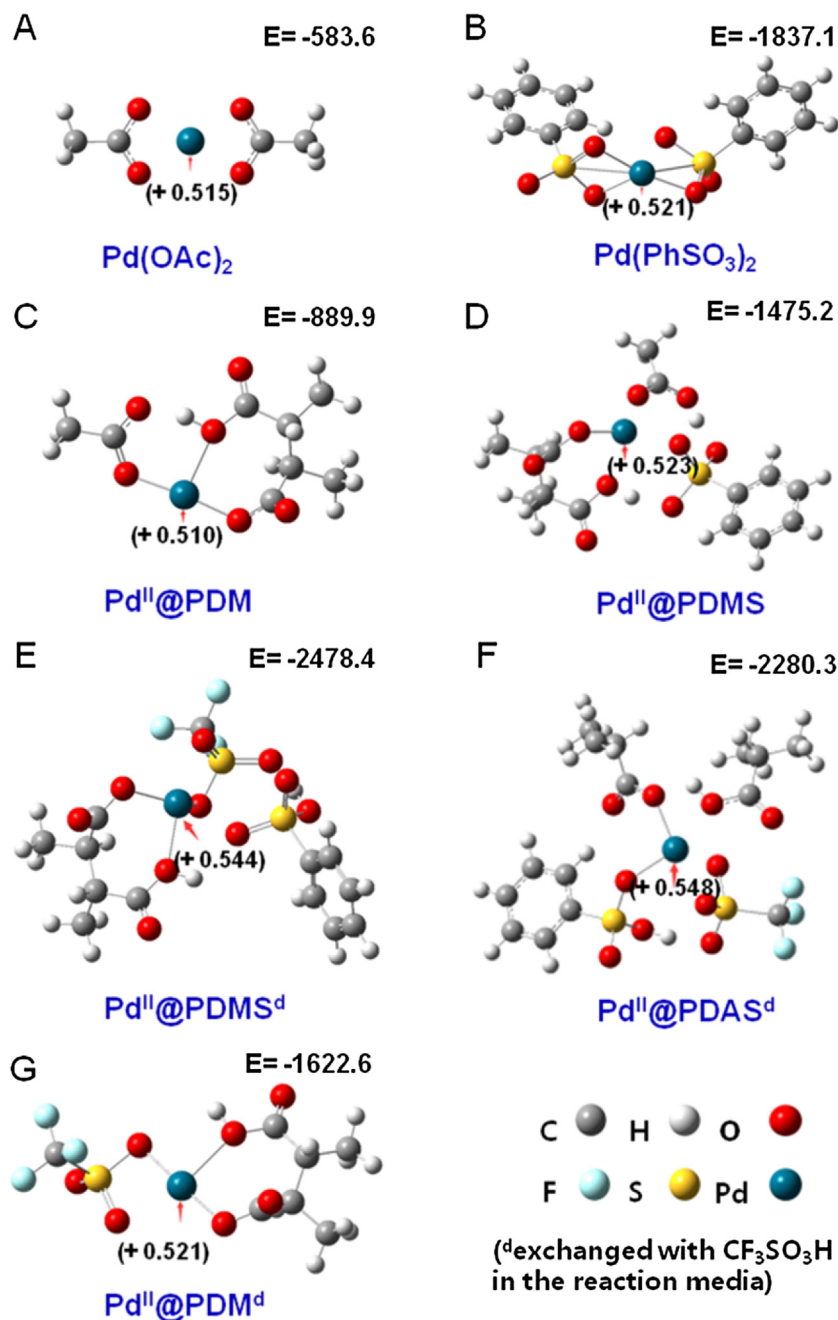
Fig. 5. Optimized geometry and corresponding energy of the repeating unit in the Pd(II) compounds simulated by DFT (energy unit in Hartree).

gle atomic Pd(II) ions to promote their stability and suppress the aggregation of Pd(0) species.

In order to verify these speculations, DFT calculations are performed to investigate the influence of the surface groups on the anchored Pd(II) ions. To simplify the calculation, simulation is carried out on the Pd(II) ions interacting with these groups in the form of free molecules of repeating units. Considering that the inevitable steric hindrance will limit the free rotation and approach of the immobilized surface groups to these Pd(II) ions, the simulation slightly differs from the actual environment of these Pd(II) ions but can represent the influence trend of these surface groups. Corresponding optimized geometry with charge distribution and energy by DFT calculation are shown in Fig. 5. The Pd charge values in Pd(OAc)$_2$ and Pd(PhSO$_3$)$_2$ are 0.515 (Fig. 5A) and 0.521 (Fig. 5B), respectively, suggesting that Pd(II) species will become more elec-

trophilic by interacting with −SO$_3$H groups. In addition, the Pd charge value is increased from 0.510 when Pd(II) ion interacts with only −COOH groups (the simulation of Pd(II) ions in Pd^{II}@PDM, Fig. 5C) to 0.523 when PhSO$_3$H groups are introduced (the simulation of Pd(II) ions in Pd^{II}@PDMS, Fig. 5D). Moreover, this value further increases to 0.544 as the (OAc)$^+$ is replaced with (O$_3$SCF$_3$)$^+$ (Fig. 5E), and it is higher than the one in Pd^{II}@PDM^d. This variation implies that the Pd(II) species interacting with these groups become more electrophilic. The formed highly electrophilic Pd(II) species Pd^{II}@PDMS^d correspond to the high performance in the reaction. Pd^{II}@PDAS^d (Fig. 5F) also exhibits high charge value close to the one in Pd^{II}@PDMS^d, but shows inferior activity due to the formation of Pd(0) species. The Pd(II) species interacting with the adjacent −COOH groups present lower energy (Fig. 5C) than the one in Pd(OAc)$_2$ (Fig. 5A), validating the stabilization effect of the adjacent

−COOH groups by forming seven-membered ring structure, which is further confirmed by the energy difference between Pd^{II}@PDMS^d (Fig. 5E) and Pd^{II}@PDAS^d (Fig. 5F). This phenomenon directs that the Pd(II) loading is a thermodynamic process (Fig. S17). Further decreased energy is observed over Pd^{II}@PDMS (Fig. 5D), suggesting the more stable structure due to the co-presence of −SO$_3$H groups, which is revealed by the lower energy of Pd^{II}@PDMS^d (Fig. 5E) than the one of Pd^{II}@PDM^d (Fig. 5G). The lowest energy is observed over Pd^{II}@PDMS^d, implying that the formation of such species is also a thermodynamic process. All of these demonstrate that the formed Pd(II) species in Pd^{II}@PDMS^d possess high electrophilicity and stability, which accounts for the remarkable catalysis performance.

4. Conclusion

Highly efficient single atomic Pd(II)-porous organic polymer (POP) catalyst was developed for the heterogeneous oxidative homo-coupling of benzene to biphenyl with O$_2$. This was achieved by anchoring Pd(II) ions on −COOH and −SO$_3$H tethered POP material. These surface groups enable the stable and highly electrophilic Pd species, which are critical for the activation of C−H bond in benzene. High yield and unexpected TON/TOF values are achieved and the catalyst can be facilely recovered and reused. Further, this catalyst can also efficiently catalyze the oxidative coupling of other nonactivated arenes. This work highlights the potential of constructing highly active, atomically dispersed catalysts on tailor-made POPs with controllable geometric and electronic characteristics for aerobic oxidative coupling of nonactivated arenes.

Acknowledgements

Appendix A. Supplementary data

Supplementary data associated with this article can be found, in the online version, at http://dx.doi.org/10.1016/j.apcatb.2017.03.029.

References

[1] S.A. Girard, T. Knauber, C.J. Li, Angew. Chem. Int. Ed. 53 (2014) 74–100.
[2] M. Moselage, J. Li, L. Ackermann, ACS Catal. 6 (2015) 498–525.
[3] L. Souillart, N. Cramer, Chem. Rev. 115 (2015) 9410–9464.
[4] N. Ca', M. Della, E. Fontana, M. Motti, Acc. Catellani, Chem. Res. 49 (2016) 1389–1400.
[5] S.H. Cho, J.Y. Kim, J. Kwak, S. Chang, Chem. Soc. Rev. 40 (2011) 5068–5083.
[6] G.Y. Song, F. Wang, X.W. Li, Chem. Soc. Rev. 41 (2012) 3651–3678.
[7] B.J. Li, Z.J. Shi, Chem. Soc. Rev. 41 (2012) 5588–5598.
[8] R. Kumar, E.V. Van der Eycken, Chem. Soc. Rev. 42 (2013) 1121–1146.
[9] X.H. Zhang, L.W. Chung, Y.D. Wu, Acc. Chem. Res. 49 (2016) 1302–1310.
[10] L.L. Chng, J. Zhang, J.H. Yang, M. Amoura, J.Y. Ying, Adv. Synth. Catal. 353 (2011) 2988–2998.
[11] T. Ishida, R. Tsunoda, Z.Z. Zhang, A. Hamasaki, T. Honma, H. Ohashi, T. Yokoyama, M. Tokunaga, Appl. Catal. B 150 (2014) 523–531.
[12] P. Pachfule, M.K. Panda, S. Kandambeth, S.M. Shivaprasad, D.D. Díaz, R. Banerjee, J. Mater. Chem. A 2 (2014) 7944–7952.
[13] P. Serna, A. Corma, J. Catal. 315 (2014) 41–47.
[14] T. Ishida, S. Aikawa, Y. Mise, R. Akebi, A. Hamasaki, T. Honma, H. Ohashi, T. Tsuji, Y. Yamamoto, M. Miyasaka, M. Yokoyama, M. Tokunaga, ChemSusChem 8 (2015) 695–701.
[15] C.L. Sun, B.J. Li, Z.J. Shi, Chem. Commun. 46 (2010) 677–685.
[16] M.R. Haneline, M. Tsunoda, F.P. Gabbaï, J. Am. Chem. Soc. 124 (2002) 3737–3742.
[17] P. Lloyd-Williams, E. Giralt, Chem. Soc. Rev. 30 (2001) 145–157.
[18] M. Lemaire, Chem. Rev. 102 (2002) 1359–1470.
[19] S. Mukhopadhyay, G. Rothenberg, G. Lando, K. Agbaria, M. Kazanci, Y. Sasson, Adv. Synth. Catal. 343 (2001) 455–459.
[20] T. Yokota, S. Sakaguchi, Y. Ishii, Adv. Synth. Catal. 344 (2002) 849–854.
[21] P.P. Zhao, Y. Leng, M.J. Zhang, J. Wang, Y.J. Wu, J. Huang, Chem. Commun. 48 (2012) 5721–5723.
[22] Y.Q. Liu, X.C. Wang, X.C. Cai, G.J. Chen, J. Li, Y. Zhou, J. Wang, ChemCatChem 8 (2016) 448–454.
[23] B.T. Qiao, A.Q. Wang, X.F. Yang, L.F. Allard, Z. Jiang, Y.T. Cui, J.Y. Liu, J. Li, T. Zhang, Nat. Chem. 3 (2011) 634–641.
[24] X.F. Yang, A.Q. Wang, B.T. Qiao, J. Li, J.Y. Liu, T. Zhang, Acc. Chem. Res. 46 (2013) 1740–1748.
[25] H. Duan, M.H. Li, G.H. Zhang, J.R. Gallagher, Z.L. Huang, Y. Sun, Z. Luo, H.Z. Chen, J.T. Miller, R.Q. Zou, A.W. Lei, Y.L. Zhao, ACS Catal. 5 (2015) 3752–3759.
[26] J.D. Kistler, N. Chotigkrai, P.H. Xu, B. Enderle, P. Praserthdam, C.Y. Chen, N.D. Browning, B.C. Gates, Angew. Chem. Int. Ed. 126 (2014) 9050–9053.
[27] F.R. Lucci, J.L. Liu, M.D. Marcinkowski, M. Yang, L.F. Allard, M. Flytzani-Stephanopoulos, E.C.H. Sykes, Nat. Commun. 6 (2015) 8550.
[28] C. Coperet, A. Comas-Vives, M.P. Conley, D.P. Estes, A. Fedorov, V. Mougel, H. Nagae, P.A. Zhizhko, Chem. Rev. 116 (2016) 323–421.
[29] B. Zhang, H. Asakura, J. Zhang, J.G. Zhang, S. De, N. Yan, Angew. Chem. Int. Ed. 55 (2016) 1–6.
[30] P.X. Liu, Y. Zhao, R.X. Qin, S.G. Mo, G.X. Chen, L. Gu, D.M. Chevrier, P. Zhang, Q. Guo, D.D. Zang, B.H. Wu, G. Fu, N.F. Zheng, Science 352 (2016) 797–800.
[31] J. Jones, H.F. Xiong, A.T. DeLaRiva, E.J. Peterson, H. Pham, S.R. Challa, G. Qi, S. Oh, M.H. Wiebenga, X.I.P. Hernández, Y. Wang, A.K. Abhaya, K. Datye, Science 353 (2016) 150–154.
[32] W.G. Liu, L.L. Zhang, W.S. Yan, X.Y. Liu, X.F. Yang, S. Miao, W.T. Wang, A.Q. Wang, T. Zhang, Chem. Sci. 7 (2016) 5758–5764.
[33] J.L. Liu, F.R. Lucci, M. Yang, S. Lee, M.D. Marcinkowski, A.J. Therrien, C.T. Williams, E.C.H. Sykes, M. Flytzani-Stephanopoulos, J. Am. Chem. Soc. 138 (2016) 6396–6399.
[34] Y. Izawa, S.S. Stahl, Adv. Synth. Catal. 352 (2010) 3223–3229.
[35] A. Thomas, Angew. Chem. Int. Ed. 49 (2010) 8328–8344.
[36] Y.G. Zhang, S.N. Riduan, Chem. Soc. Rev. 41 (2012) 2083–2094.
[37] Y.H. Xu, S.B. Jin, H. Xu, A. Nagai, D.L. Jiang, Chem. Soc. Rev. 42 (2013) 8012–8031.
[38] K. Sakaushi, M. Antonietti, Acc. Chem. Res. 48 (2015) 1591–1600.
[39] X.C. Wang, Y. Zhou, Z.J. Guo, G.J. Chen, J. Li, Y.M. Shi, Y.Q. Liu, J. Wang, Chem. Sci. 6 (2015) 6916–6924.
[40] A.G. Slater, A.I. Cooper, Science 348 (2015) aaa8075.
[41] A.R. Khokhar, G.J. Lumetta, Inorg. Chim. Acta. 153 (1988) 255–259.
[42] B. Ravel, M.A.T.H.E.N.A.J. Newville, Synchrotron Radiat. 12 (2005) 537–541.
[43] M.J. Frisch, G.W. Trucks, H.B. Schlegel, G.E. Scuseria, M.A. Robb, J.R. Cheeseman, G. Scalmani, V. Barone, B. Mennucci, G.A. Petersson, H. Nakatsuji, M. Caricato, X. Li, H.P. Hratchian, A.F. Izmaylov, J. Bloino, G. Zheng, J.L. Sonnenberg, M. Hada, M. Ehara, K. Toyota, R. Fukuda, J. Hasegawa, M. Ishida, T. Nakajima, Y. Honda, O. Kitao, H. Nakai, T. Vreven, J.A. Montgomery Jr., J.E. Peralta, F. Ogliaro, M. Bearpark, J.J. Heyd, E. Brothers, K.N. Kudin, V.N. Staroverov, T. Keith, R. Kobayashi, J. Normand, K. Raghavachari, A. Rendell, J.C. Burant, S.S. Iyengar, J. Tomasi, M. Cossi, N. Rega, J.M. Millam, M. Klene, J.E. Knox, J.B. Cross, V. Bakken, C. Adamo, J. Jaramillo, R. Gomperts, R.E. Stratmann, O. Yazyev, A.J. Austin, R. Cammi, C. Pomelli, J.W. Ochterski, R.L. Martin, K. Morokuma, V.G. Zakrzewski, G.A. Voth, P. Salvador, J.J. Dannenberg, S. Dapprich, A.D. Daniels, O. Farkas, J.B. Foresman, J.V. Ortiz, J. Cioslowski, D.J. Fox, 09 Gaussian, Revision D.01, Gaussian Inc, Wallingford, CT, 2013.
[44] B. Mutz, H.W. Carvalho, S. Mangold, W. Kleist, J.D. Grunwaldt, J. Catal. 327 (2015) 48–53.
[45] A.M. Gänzler, M. Casapu, A. Boubnov, O. Müller, S. Conrad, H. Lichtenberg, R. Frahm, J.D. Grunwaldt, J. Catal. 328 (2015) 216–224.
[46] X.Q. Jia, S.H. Wang, Y. Fan, J. Catal. 327 (2015) 54–57.
[47] B.I.R.G.I.T. Nyberg, R.A.G.N.A.R. Larsson, Acta Chem. Scand. 27 (1973) 63–70.
[48] Y.Y. Liu, K. Murata, M. Inaba, J. Mol. Catal. A: Chem. 256 (2006) 247–255.
[49] P.H. Xi, F. Yang, S. Qin, D.B. Zhao, J.B. Lan, G. Gao, C.W. Hu, J.S. You, J. Am. Chem. Soc. 132 (2010) 1822–1824.
[50] I. Hussain, T. Singh, Adv. Synth. Catal. 356 (2014) 1661–1696.
[51] J.E. Lyons, in: A.E. Martell, D.T. Sawyer (Eds.), In Oxygen Complexes and Oxygen Activation by Transition Metal Complexes, Plenum Press, New York, 1988, pp. 233–251 (and references therein.).
[52] D. Wang, Y. Izawa, S.S. Stahl, J. Am. Chem. Soc. 136 (2014) 9914–9917.